Momentum-exchange method in lattice Boltzmann simulations of particle-fluid interactions

Yu Chen,[1] Qingdong Cai,[2] Zhenhua Xia,[2] Moran Wang,[1,*] and Shiyi Chen[2]
[1]*Department of Engineering Mechanics, School of Aerospace, Tsinghua University, Beijing 100084, China*
[2]*LTCS, CAPT, and Department of Mechanics and Aerospace Engineering, Peking University, Beijing 100871, China*
(Received 14 May 2013; published 8 July 2013)

The momentum exchange method has been widely used in lattice Boltzmann simulations for particle-fluid interactions. Although proved accurate for still walls, it will result in inaccurate particle dynamics without corrections. In this work, we reveal the physical cause of this problem and find that the initial momentum of the net mass transfer through boundaries in the moving-boundary treatment is not counted in the conventional momentum exchange method. A corrected momentum exchange method is then proposed by taking into account the initial momentum of the net mass transfer at each time step. The method is easy to implement with negligible extra computation cost. Direct numerical simulations of a single elliptical particle sedimentation are carried out to evaluate the accuracy for our method as well as other lattice Boltzmann-based methods by comparisons with the results of the finite element method. A shear flow test shows that our method is Galilean invariant.

DOI: 10.1103/PhysRevE.88.013303 PACS number(s): 47.11.−j, 47.55.Kf, 02.70.−c

I. INTRODUCTION

Efficient and accurate simulation of particle-fluid interactions plays an important role in many industrial situations, such as petroleum, chemical engineering, earth, and environmental processes [1–4]. Compared with the finite element method (FEM), which requires continuously regeneration of body-fitting mesh, direct simulation of particle-fluid interactions using the lattice Boltzmann (LB) method is more efficient [5], especially for a large number of particles.

A moving boundary condition and evaluation of the hydrodynamic force on the solid object are the two major challenges in LB simulations of particle-fluid interactions. Particle suspension models are primary targeted to solve the above two challenges, which can be divided into two categories by either excluding fluid information inside the particle or not. The most popular models include the shell model by Ladd [6,7] and the ALD (Aidun, Lu, and Ding) method by Aidun *et al.* [8].

Ladd [6,7] proposed a particle suspension model based on the midway bounce-back boundary condition. This model is actually a shell model, as fluid exists on both sides of the particle boundary. The same bounce-back operation is carried out for both interior fluid and exterior fluid. The momentum exchange method based on the difference of distribution functions from opposite directions along the boundary link is proposed to evaluate the hydrodynamic force acting on the particle. For the shell model, both interior fluid and exterior fluid contribute in the momentum exchange calculation. As a result, the particle motion may be affected by the interior fluid, and the model is limited to relatively heavy particles if explicit update of the particle dynamics is employed [6–10]. Although the implicit update scheme can relax the restriction of heavy particles [10,11], the shell model may still have difficulties in certain situations such as employing interpolation-based curved boundary conditions or simulating particle suspensions in a multicomponent fluid [12].

Aidun *et al.* [8] excludes the interior fluid used in Ladd's shell model, and the momentum exchange calculation now involves only the exterior fluid. In addition, an impulse force is proposed to apply to the particle whenever the particle moves to cover or uncover a lattice node. The physical meaning of this impulse force has not been well explained, and the use of this impulse force is also questioned [13]. Once the impulse force is applied, the total fluid force acting on the particle fluctuates significantly, which may reduce the stability of the simulation. Wen *et al.* [14] confirm that this impulse force is necessary to obtain correct particle dynamics for the nonshell particle model.

During the last two decades, several interpolation-based curved boundary conditions have been developed [15–18]. Compared with the midway bounce-back boundary condition, these curved boundary conditions are second-order accurate for arbitrary surface and ensure smoother force transition when the particle moves. The curved boundary conditions have been applied to LB simulations of particle-fluid interactions [5,14,19–21]. The interior fluid is excluded in these simulations, and force evaluation is via the stress integration method [5,19,20] or the momentum exchange method with the impulse force correction [14,21].

The stress integration method requires a huge amount of extrapolations of fluid information off grid and becomes even more complex and costly in three-dimensional simulations. The conventional momentum exchange method is easy to implement and has high efficiency; however, the benefit of curved boundary conditions may be compromised if the impulse force is applied, which results in a fluctuating hydrodynamic force on the particle. In this paper we reveal the physical cause of the inaccurate particle dynamics obtained by using the conventional momentum exchange method without correction, which is also responsible for breaking Galilean invariance. A simple corrected momentum exchange method is then proposed, and the impulse force is no longer required. As a result, the simplicity of the momentum exchange method

*mrwang@tsinghua.edu.cn

remains, and the force obtained by our method is as smooth as the force by the stress integration method. Numerical simulations of sedimentation of a single elliptical particle are carried out to evaluate different lattice Boltzmann-based methods, and simulation results of the finite element method are adopted for comparison. A shear flow test is also performed to examine the Galilean invariance of these methods.

The rest of the paper is organized as follows. Section II introduces the numerical algorithms for particle-fluid interactions, including a brief review of the lattice Boltzmann method, nonslip boundary treatments, force evaluation methods, and particle dynamics. Numerical simulations of sedimentation of a single elliptical particle are carried out to demonstrate problems and difficulties of the existing lattice Boltzmann-based methods in Sec. III. In Sec. IV we propose a corrected momentum exchange method. Numerical validation of our new method will be provided in Sec. V, as well as further evaluation of other lattice Boltzmann-based methods. Section VI concludes the paper.

II. NUMERICAL METHODS FOR PARTICLE SUSPENSIONS

A. Lattice Boltzmann method

The main variable in LBM is the discretized velocity distribution function f_i, and the governing equation with the popular BGK model [22–25] is

$$f_i(\boldsymbol{x}+\boldsymbol{e}_i\delta t,t+\delta t)=f_i(\boldsymbol{x},t)-\frac{f_i(\boldsymbol{x},t)-f_i^{\mathrm{eq}}(\boldsymbol{x},t)}{\tau}, \tag{1}$$

where f_i is the distribution function associated with the ith discrete velocity direction $\boldsymbol{e}_i$, f_i^{eq} is the corresponding equilibrium distribution function, δt is the time increment, and τ is the relaxation time, which relates to the kinematic viscosity by

$$\nu=(\tau-1/2)c_s^2\delta t, \tag{2}$$

where c_s is the speed of sound. For the two-dimensional, nine-speed LB model (D2Q9) [22], we have

$$\mathbf{e}_i=\begin{cases}0, & i=0\\ c(\cos[(i-1)\pi/4],\sin[(i-1)\pi/4]), & i=1,3,5,7\\ c(\sqrt{2}\cos[(i-1)\pi/4],\sqrt{2}\sin[(i-1)\pi/4]), & i=2,4,6,8,\end{cases} \tag{3}$$

where $c=\delta x/\delta t$ and δx is the lattice spacing. The equilibrium distribution is

$$f_i^{\mathrm{eq}}(\rho,\mathbf{u})=\rho w_i\left[1+\frac{\mathbf{e}_i\cdot\mathbf{u}}{3c^2}+\frac{9(\mathbf{e}_i\cdot\mathbf{u})^2}{2c^4}-\frac{3\mathbf{u}\cdot\mathbf{u}}{2c^2}\right], \tag{4}$$

where $w_0=4/9$, $w_i=1/9$, for $i=1,3,5,7$, and $i=1/36$, for $i=2,4,6,8$. For simplicity, we set c, δx, and δt to be unity in the rest of the paper. The macroscopic density and momentum density are defined as

$$\rho=\sum_i f_i, \tag{5}$$

$$\rho\mathbf{u}=\sum_i f_i\mathbf{e}_i. \tag{6}$$

The pressure is obtained by

$$p=c_s^2\rho. \tag{7}$$

B. Nonslip boundary treatments

In this paper we mainly focus on the link-based nonslip boundary conditions, which are most widely used in LB simulations of particle-fluid interactions. Figure 1 shows the typical link-based boundary model. In link-based boundary models, fluid interacts with solid through boundary links, such as link AC in Fig. 1, which connects a fluid node A and a solid node C.

Classic particle suspension models employ the midway bounce-back boundary condition, as it is very easy to implement and requires no interpolations or extrapolations, which becomes critical when particles are densely packed as there may not be sufficient fluid information available for interpolations or extrapolations. The midway bounce-back means that fluid particles traveling from a fluid node towards a solid node will be bounced back on the midpoint of the boundary link, such as point E in Fig. 1, regardless of the physical position of the wall. If the wall is still, then the bounce-back procedure is

$$f_{\bar{\alpha}}(\boldsymbol{x}_f,t+\Delta t)=\tilde{f}_\alpha(\boldsymbol{x}_f,t), \tag{8}$$

where $\boldsymbol{x}_f$ is the location of the fluid node just outside the solid surface as shown in Fig. 1, $\boldsymbol{e}_\alpha$ is the lattice direction from a

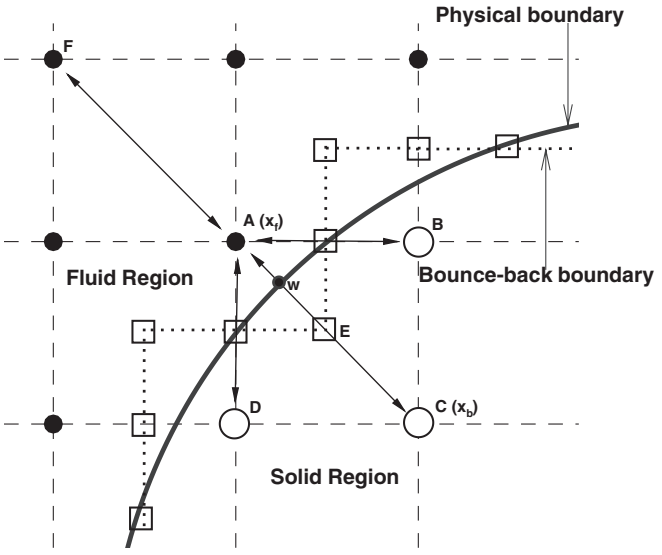

FIG. 1. A schematic illustration of link-based lattice Boltzmann boundary model.

fluid node to solid node, $\boldsymbol{e}_{\bar{\alpha}}$ is the opposite direction, and $\tilde{f}$ is the postcollision distribution function. If the wall is moving, then an additional term is added into Eq. (8) [6]:

$$f_{\bar{\alpha}}(\boldsymbol{x}_f,t+\Delta t) = \tilde{f}_{\alpha}(\boldsymbol{x}_f,t) - 2\omega_{\alpha}\rho\frac{\boldsymbol{e}_{\alpha}\cdot\boldsymbol{u}_w}{c_s^2}, \tag{9}$$

where $\boldsymbol{u}_w$ is evaluated on the midpoint of the boundary link. The drawback of the midway bounce-back boundary condition is that the resulting nonslip boundary is a zigzag-type boundary as shown in Fig. 1 and is only first-order accurate for arbitrary surface. If accurate particle dynamics is the primary objective, and the particles are not densely packed, higher-order interpolation-based curved boundary conditions should be employed instead of the midway bounce-back boundary condition.

The main idea of the curved boundary conditions is to take the exact wall position (point W in Fig. 1) into consideration and interpolate required information from nearby fluid nodes. In this paper we employ the curved boundary condition proposed by Mei *et al.* [16,26]. However, the new momentum exchange method proposed in Sec. IV is not limited to the curved boundary condition used in this paper. The formula of Mei's curved boundary condition is

$$\tilde{f}_{\bar{\alpha}}(\boldsymbol{x}_b,t) = (1-\chi)\tilde{f}_{\alpha}(\boldsymbol{x}_f,t) + \chi f_{\alpha}^{(*)}(\boldsymbol{x}_b,t) - 2\omega_{\alpha}\rho\frac{\boldsymbol{e}_{\alpha}\cdot\boldsymbol{u}_w}{c_s^2}, \tag{10}$$

where $\boldsymbol{x}_b$ is the solid node just inside the solid surface as shown in Fig. 1, and $f_{\alpha}^{(*)}(\boldsymbol{x}_b,t)$ is obtained by

$$f_{\alpha}^{(*)}(\boldsymbol{x}_b,t) = \omega_{\alpha}\rho(\boldsymbol{x}_f,t)\left[1+\frac{1}{c_s^2}\boldsymbol{e}_{\alpha}\cdot\boldsymbol{u}_{bf}+\frac{1}{2c_s^4}(\boldsymbol{e}_{\alpha}\cdot\boldsymbol{u}_f)^2-\frac{1}{2c_s^2}\boldsymbol{u}_f\cdot\boldsymbol{u}_f\right]. \tag{11}$$

Differently from the midway bounce-back condition, $\boldsymbol{u}_w$ is evaluated on the exact intersecting point of the boundary link and the physical wall. $\boldsymbol{u}_f = \boldsymbol{u}(\boldsymbol{x}_f,t)$ is the fluid velocity near the wall, and $\boldsymbol{u}_{bf}$ is given by [26]

$$\boldsymbol{u}_{bf} = \begin{cases} (\Delta-1.5)\boldsymbol{u}_f/\Delta,\ \chi=(2\Delta-1)/(\tau+0.5) & \text{for} \quad \Delta \geqslant 0.5 \\ \boldsymbol{u}_{ff},\ \chi=(2\Delta-1)/(\tau-2) & \text{for} \quad \Delta \leqslant 0.5, \end{cases} \tag{12}$$

where $\boldsymbol{u}_{ff} = \boldsymbol{u}(\boldsymbol{x}_f-\boldsymbol{e}_{\alpha},t)$, and Δ is the fraction of an intersected link in the fluid region:

$$\Delta = \frac{|\boldsymbol{x}_f-\boldsymbol{x}_w|}{|\boldsymbol{x}_f-\boldsymbol{x}_b|}. \tag{13}$$

C. Force evaluation methods

To obtain accurate hydrodynamic force and torque on the solid object immersed in a fluid flow is a matter of critical importance. There are mainly two kinds of force evaluation methods used in lattice Boltzmann simulations, namely, the momentum exchange method and the stress integration method [27].

1. Momentum exchange method

The momentum exchange (ME) method is unique to LBM. First proposed by Ladd [6], this method is very simple and easy to implement. The hydrodynamic force acting on the solid surface is obtained by calculating the momentum exchange on each boundary link (as shown in Fig. 1):

$$\delta\boldsymbol{F}_w(\boldsymbol{x}_w,\boldsymbol{e}_{\alpha}) = -[f_{\bar{\alpha}}(\boldsymbol{x}_f,t)\boldsymbol{e}_{\bar{\alpha}} - \tilde{f}_{\alpha}(\boldsymbol{x}_f,t)\boldsymbol{e}_{\alpha}]. \tag{14}$$

The total hydrodynamic force on a solid object is the sum of $\delta\boldsymbol{F}_w(\boldsymbol{x}_w,\boldsymbol{e}_{\alpha})$ computed from each boundary link of the solid object surface:

$$\boldsymbol{F}_w = \sum \delta\boldsymbol{F}_w(\boldsymbol{x}_w,\boldsymbol{e}_{\alpha}), \tag{15}$$

and the total torque is

$$\boldsymbol{T}_w = \sum (\boldsymbol{x}_w-\boldsymbol{R})\times\delta\boldsymbol{F}_w(\boldsymbol{x}_w,\boldsymbol{e}_{\alpha}), \tag{16}$$

where $\boldsymbol{R}$ is the mass center of the solid object. In Ladd's shell model [6], $\boldsymbol{F}_w$ is the sum of the momentum exchange from both exterior fluid and interior fluid:

$$\boldsymbol{F}_w = \boldsymbol{F}_w^{\text{interior}} + \boldsymbol{F}_w^{\text{exterior}}. \tag{17}$$

2. Stress integration method

For the stress integration (SI) method, the hydrodynamic force on a solid object is obtained by integration of the stresses on the surface ($\partial\Omega$) of the object:

$$\boldsymbol{F}_w = \int_{\partial\Omega}\boldsymbol{\sigma}\cdot\boldsymbol{n}\,dS, \tag{18}$$

and the torque on the object is

$$\boldsymbol{T}_w = \int_{\partial\Omega}\boldsymbol{r}\times(\boldsymbol{\sigma}\cdot\boldsymbol{n})\,dS, \tag{19}$$

where $\boldsymbol{n}$ is a unit outward normal vector on the object surface $\partial\Omega$ and $\boldsymbol{r}$ is a vector from the center of the object to $\partial\Omega$. The stress tensor $\boldsymbol{\sigma}$ for two-dimensional incompressible flow can be expressed as

$$\sigma_{ij} = -p\delta_{ij} + \rho\nu(\partial_i u_j + \partial_j u_i). \tag{20}$$

In Eq. (20), pressure p is known to us as provided by Eq. (7). In order to avoid computing the macroscopic velocity gradient, Mei *et al.* [28] propose the following formula to calculate the stress:

$$\sigma_{ij} = -p\delta_{ij} - \left(1-\frac{1}{2\tau}\right)\Sigma_{\alpha}\left[f_{\alpha}-f_{\alpha}^{\text{eq}}\right] \times\left(e_{\alpha,i}e_{\alpha,j}-\frac{1}{2}\boldsymbol{e}_{\boldsymbol{\alpha}}\cdot\boldsymbol{e}_{\boldsymbol{\alpha}}\delta_{ij}\right). \tag{21}$$

Inamuro *et al.* [29] propose a different form of σ_{ij} based on asymptotic analysis. The difference between the simulation results of the two forms is very small, and we present only

the results of Eq. (21) in the rest of the paper. The fluid distribution functions in Eq. (21) are evaluated on the physical surface $\partial\Omega$; thus, extrapolations from nearby fluid lattice nodes are required. In this work, we follow the extrapolation scheme introduced by Li *et al.* [19] to compute the distribution functions on $\partial\Omega$.

The midway bounce-back boundary condition results in a zigzag nonslip surface, which is different from the physical solid surface. In this case, stress integration on the physical surface may cause significant error. Inamuro *et al.* [29] suggest integrating the stress on a slightly larger surface which is apart from the physical one. However, due to the high computation cost of the SI method compared to the boundary condition treatment, it is not reasonable to apply the midway bounce-back boundary condition when the SI method is adopted for force evaluation. When the curved boundary condition is applied, the resulting nonslip surface and the physical surface should coincide, and the integration surface $\partial\Omega$ used in Eqs. (18) and (19) is the physical surface.

D. Particle dynamics

The motion of a particle is obtained by solving Newton's equations [8]:

$$M\frac{d\boldsymbol{U}(t)}{dt} = \boldsymbol{F}_w + \boldsymbol{f}, \tag{22}$$

$$\boldsymbol{I}\cdot\frac{d\boldsymbol{\Omega}(t)}{dt} + \boldsymbol{\Omega}(t)\times[\boldsymbol{I}\cdot\boldsymbol{\Omega}(t)] = \boldsymbol{T}_w, \tag{23}$$

where $\boldsymbol{f}$ is the body force, such as gravity.

In Ladd's shell model, an effective shell mass $M_e = M_s - M_{\text{interior}}$ should be used to update the particle motion in Eqs. (22) and (23), where M_s denotes the mass of the real solid particle and M_{interior} denotes the mass of the fluid inside the shell. As a result, for explicit update of particle motion, the solid-fluid density ratio is constrained by [3,9]

$$\frac{\rho_s}{\rho_f} > 1 + \frac{10}{r}, \tag{24}$$

which limits the use of the shell model.

For particle suspension model without interior fluid, some lattice nodes originally inside the solid particle will enter the fluid region when the particle moves. In this case, fluid information in these newly created fluid lattice nodes has to be extrapolated from nearby fluid nodes. Here we use the same extrapolation method based on the direct extrapolation of distribution functions introduced in Ref. [5].

Aidun *et al.* [8] suggest an impulse force should be applied to the particle whenever the particle moves to cover or uncover a lattice node, as the fluid momentum of the corresponding node is gained or lost by the particle, respectively:

$$\sum_{CN}\boldsymbol{F}_c(\boldsymbol{x}_{\text{cover}}) = \sum_{CN}\rho\boldsymbol{U}, \tag{25}$$

$$\sum_{CN}\boldsymbol{T}_c(\boldsymbol{x}_{\text{cover}}) = \sum_{CN}[\boldsymbol{x}_{\text{cover}} - \boldsymbol{R}]\times\boldsymbol{F}_c(\boldsymbol{x}_{\text{cover}}), \tag{26}$$

$$\sum_{UN}\boldsymbol{F}_u(\boldsymbol{x}_{\text{uncover}}) = -\sum_{UN}\rho\boldsymbol{U}, \tag{27}$$

$$\sum_{UN}\boldsymbol{T}_u(\boldsymbol{x}_{\text{uncover}}) = \sum_{UN}[\boldsymbol{x}_{\text{uncover}} - \boldsymbol{R}]\times\boldsymbol{F}_u(\boldsymbol{x}_{\text{uncover}}), \tag{28}$$

where CN and UN denote lattice nodes being covered or uncovered by the particle during one time step, respectively.

There is still lack of detailed interpretation of the above impulse force, which may cause confusion about the use of the impulse force. Furthermore, the impulse force may reduce the stability of simulation, especially when the particle is much lighter than the fluid. When the higher-order curved boundary condition is employed, the force and torque are evaluated on the exact intersecting point of the boundary link and the physical wall in the ME method. Thus, one may argue that the above impulse force may be unnecessary in this case. However, simulation results of Wen *et al.* [14] confirm that the impulse force is necessary to obtain correct particle dynamics even when the curved boundary condition is employed, if force evaluation is via the momentum exchange method. In Sec. III we also perform simulations of sedimentation of a single elliptical particle to examine the necessity of the impulse force.

III. PROBLEMS FOUND IN THE NUMERICAL SIMULATION OF SEDIMENTATION OF A SINGLE ELLIPTICAL PARTICLE

Direct numerical simulations of particle sedimentation have been presented in many papers [3,5,30–32], using either the finite element method or the lattice Boltzmann method. Thus, there are sufficient data available for benchmark comparison. The benchmark case used in Ref. [5], numerical simulation of the settling process of a single elliptical particle in a long channel, is chosen to evaluate the accuracy of different methods introduced in Sec. II. There are mainly three reasons why we choose this case for benchmark comparison. First, there are available simulation results obtained by both the finite element method and the lattice Boltzmann method for comparison [5]; second, elliptical particle is more sensitive to simulation errors compared to a circular particle; and, third, direct numerical simulation of particle sedimentation is also of practical importance [5,30].

Table I shows the notations for different lattice Boltzmann-based methods used in this paper. Although the link-based boundary conditions are most widely used in LB simulations of particle-fluid interactions, several node-based models have also been developed [33,34], in which the fluid-solid coupling is through the direct alteration of fluid nodes adjacent to the solid surface [1], and it is worth comparing the node-based models with the link-based models. Thus, a volume fraction LB model proposed by Nobel and Torczynski [33], one of the node-based models, is also added in the benchmark simulations, denoted as VF as shown in Table I. In the VF model, like Ladd's shell model, fluid exists in the whole computation domain, including the solid region, and, instead of an explicit boundary treatment, the collision term in the LB governing equation, Eq. (1), is modified according to the solid volume fraction of a lattice cell to distinguish the solid phase and the fluid phase. Force evaluation is based on the momentum transfer that occurs over the lattice nodes covered by solid [35], which is unique to the VF model.

The geometry of the benchmark case is shown in Fig. 2. a and b are the length of the semimajor axis and semiminor axis, respectively. L is the width of the channel. Gravity is along the

TABLE I. Notations for different lattice Boltzmann-based methods used in this paper.

Method	Boundary condition	Force evaluation	Impulse force	Interior fluid
CB-SI	Curved boundary	Stress integration	No	No
CB-SI-IMP	Curved boundary	Stress integration	Yes	No
CB-ME	Curved boundary	Momentum exchange	No	No
CB-ME-IMP	Curved boundary	Momentum exchange	Yes	No
BB-SI	Midway bounce-back	Stress integration	No	No
BB-ME	Midway bounce-back	Momentum exchange	No	No
BB-ME-IMP	Midway bounce-back	Momentum exchange	Yes	No
BB-ME-shell	Midway bounce-back	Momentum exchange	No	Yes
VF	LB volume fraction model [33]		No	Yes

x axis in the positive direction. θ represents the orientation of the particle. In physical units, $a = 2b = 0.05$ cm, L is 0.4 cm, gravity is 9.8 m/s^2, and the kinematic viscosity of the fluid is 1.0×10^{-6} m^2/s. The density ratio of the solid particle and fluid is 1.1. A uniform grid with a resolution of 260 grid cells per cm is used, which is identical to the fine grid used in Ref. [5]. The relaxation time τ in Eq. (1) is set to be 0.6. The terminal particle Reynolds number is determined by the terminal settling velocity of the particle,

$$\mathrm{Re} = \frac{U_t a}{\nu}, \tag{29}$$

where U_t is the terminal velocity of the particle. In this case, the terminal particle Reynolds number is 6.6, and we will refer this sedimentation case as the Re = 6.6 case. As shown in Ref. [5], the difference between simulation results from channel with a closed wall and with an open boundary is negligible, as long as the closed channel is long enough. For simplicity, we use a closed channel in this work. The channel length is $30L$. The particle is initially placed in the middle of the channel with $\theta = 0.25\pi$ and is $3L$ away from the end of the channel in the negative direction of the x axis. We have performed simulations in a longer channel, but the difference is negligible.

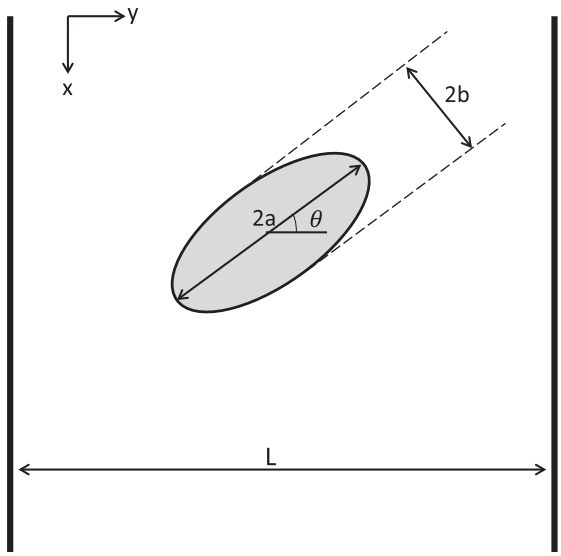

FIG. 2. The geometry of the particle sedimentation benchmark case. a and b are the length of the semimajor axis and semiminor axis, respectively. L is the width of the channel. Gravity is along the x axis in the positive direction. θ represents the orientation of the particle.

Figure 3 shows the comparison of particle trajectories and orientations obtained by FEM [5] and LBM with the curved boundary condition. CB-SI and CB-ME-IMP agree well with FEM, which is considered to be accurate. Without the impulse force correction, CB-ME deviates significantly from FEM. For the stress integration method, the impulse force should not be applied as CB-SI-IMP deviates significantly from FEM. VF also deviates from FEM in this case. Figure 4 shows the comparison of particle trajectories and orientations obtained by FEM [5] and LBM with the midway bounce-back boundary condition. Although the bounce-back boundary condition is not as accurate as the curved boundary condition, results from BB-SI and BB-ME-IMP deviate only slightly from FEM as the particle approaching to the terminal settling state in the middle of the channel when grid resolution becomes important. Similarly, without the impulse force correction, BB-ME deviates significantly from FEM.

Figure 5 shows the comparison of fluid force acting on the particle during the terminal settling state. There is no significant difference between the results from SI and ME, as long as the impulse force is not applied. However, without the impulse force correction, the trajectories and orientations obtained by CB-ME and BB-ME are inaccurate. Force obtained by LBM with the curved boundary condition is smoother than the force obtained by LBM with the midway bounce-back boundary condition. Once the impulse force is applied, force obtained by either boundary condition fluctuates significantly.

The simulation using shell model is unstable in this case, as the solid-fluid density ratio of this case is 1.1, which violates the constraint of Eq. (24). In Sec. V, a high-density ratio case will be performed to evaluate the shell model.

From the above results, we can conclude that the impulse force proposed by Aidun *et al.* [8] is necessary if the interior fluid of the particle is excluded and the ME method is used to evaluate the force on the particle, regardless of whether the midway bounce-back boundary condition or the higher-order curved boundary condition is employed. The benefit of using the curved boundary condition is compromised due to the impulse force, which results in a noisy total force, as shown in Fig. 5. When using the SI method for force evaluation, the impulse force should not be applied and the obtained force is very smooth. However, the computation cost of the SI method

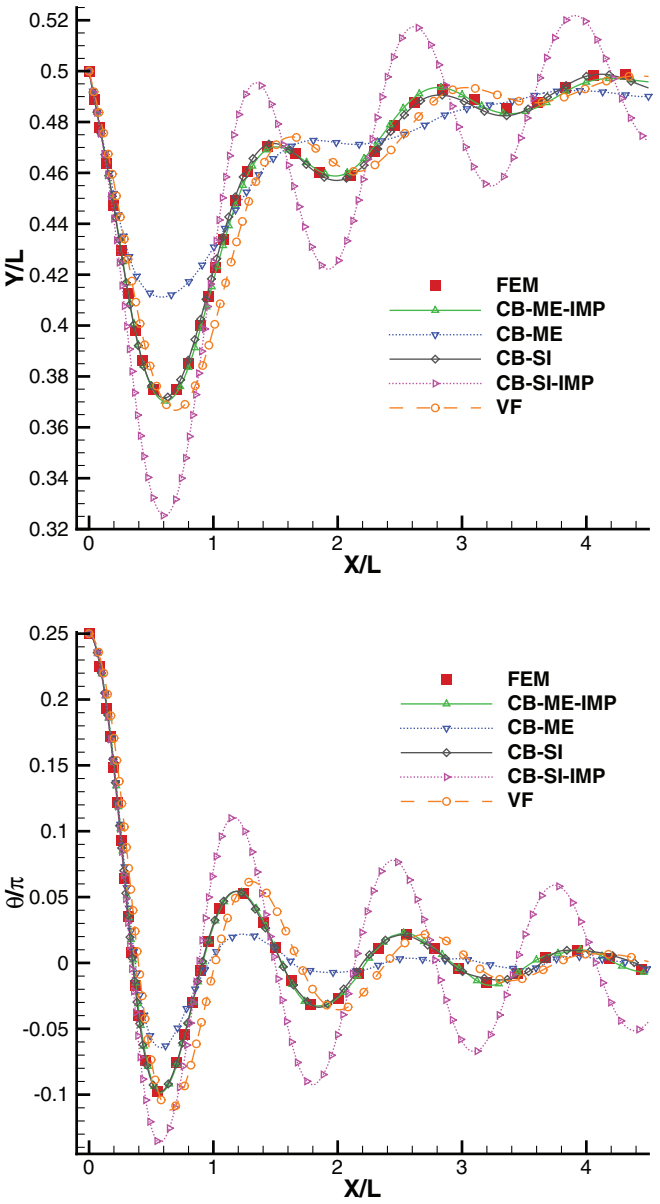

FIG. 3. (Color online) Comparison of particle trajectories and orientations for the Re = 6.6 case obtained by FEM [5] and LBM with the curved boundary condition. CB-ME, CB-SI-IMP, and VF deviate significantly from FEM, while CB-ME-IMP (with the impulse force correction) and CB-SI agree well with FEM. Thus, the impulse force proposed by Aidun *et al.* [8] is necessary to obtain correct particle dynamics if force evaluation is via the momentum exchange method, even though the curved boundary condition is employed. In contrast, for the stress integration method, the impulse force should not be applied.

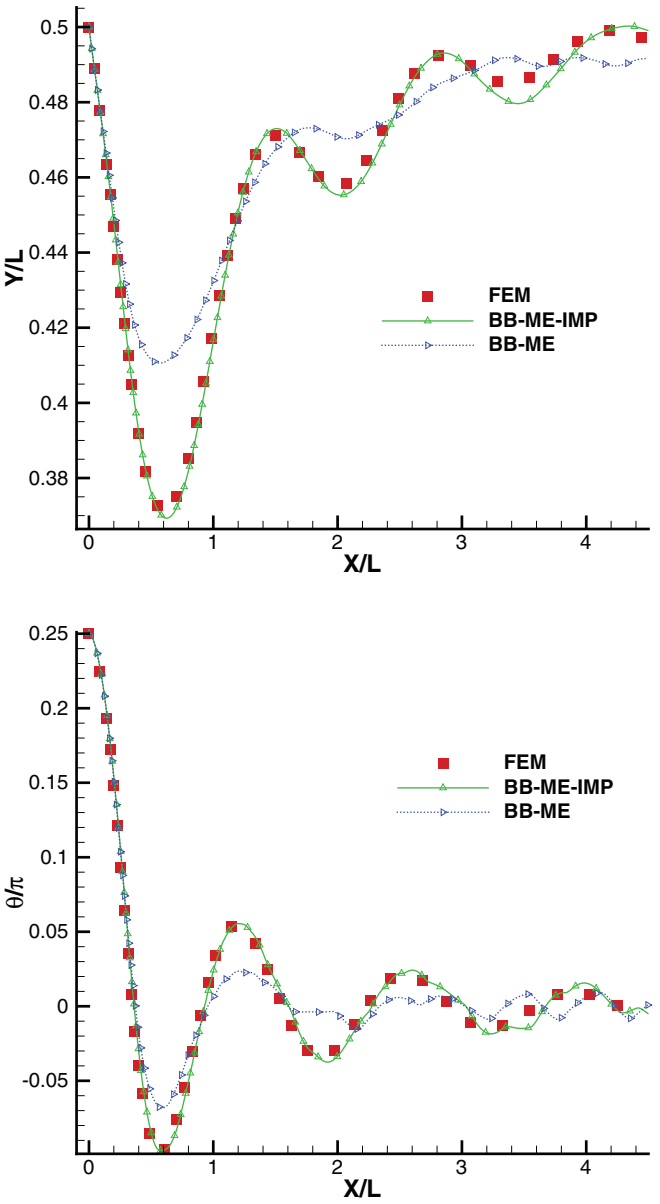

FIG. 4. (Color online) Comparison of particle trajectories and orientations for the Re = 6.6 case obtained by FEM [5] and LBM with the midway bounce-back boundary condition. BB-ME (without the impulse force correction) deviates significantly from FEM, while BB-ME-IMP (with the impulse force correction) agrees well with FEM. Thus, when the midway bounce-back boundary condition is employed, the impulse force proposed by Aidun *et al.* [8] is also necessary to obtain correct particle dynamics.

is very high compared to the ME method. Results of VF are not accurate in this particular case. Further comparisons will be performed in Sec. V.

IV. CORRECTED MOMENTUM EXCHANGE METHOD

Simulation results in Sec. III show that, for particle suspension models without interior fluid, if the impulse force proposed by Aidun *et al.* is not applied, the simulation results of LBM with the ME method deviate from both FEM results and results of LBM with the SI method. This conclusion is valid for either the midway bounce-back boundary condition or the higher-order curved boundary condition. A similar conclusion can also be found in Ref. [14]. As shown in Fig. 5, the fluid force on the particle fluctuates significantly due to the impulse force, which may reduce the simulation stability, especially for light particles.

The ME method for still walls is proved to be as accurate as the SI method [27,28]. Also, the impulse force is not required for LBM with the SI method for force evaluation.

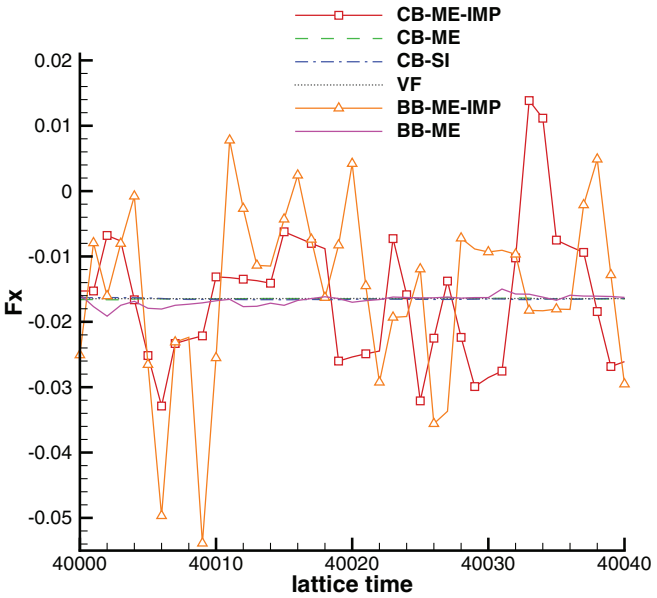

FIG. 5. (Color online) Comparison of fluid force acting on the particle during the terminal settling state for the $\mathrm{Re} = 6.6$ case obtained by LBM. When the impulse force is applied, the total fluid force obtained by CB-ME-IMP and BB-ME-IMP fluctuates significantly, which may reduce the simulation stability.

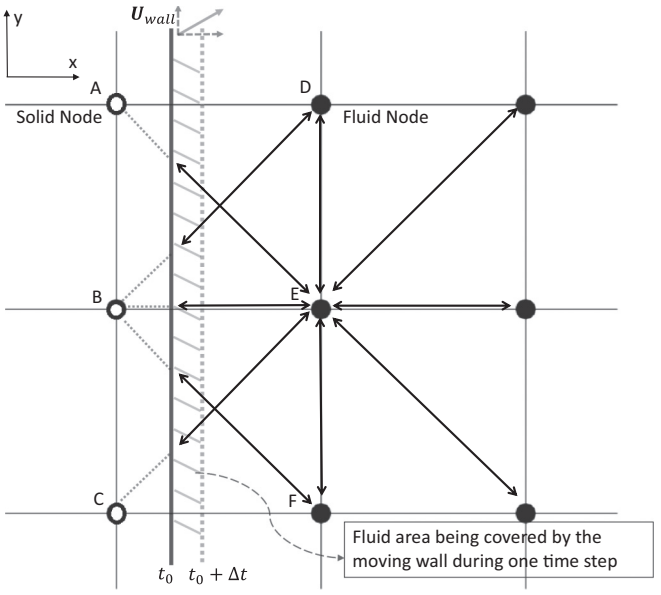

FIG. 6. A schematic illustration of a moving wall in the lattice grid.

The problem then lies in the ME calculation in the moving boundary treatment.

In LBM, the lattice velocity of fluid particles is discretized [24] and fixed during the simulation, as shown in Eq. (3). When the fluid particles collide with a still wall, the simplest way to ensure nonslip boundary condition is the bounce-back procedure. However, when the wall is moving, fluid particles colliding with the wall will gain additional momentum due to the moving wall. Since the lattice velocity of the fluid particle is fixed, the additional momentum has to be adjusted by modifying the reflected distribution function in the bounce-back procedure, as shown in Eq. (9), which results in a net mass transfer through the physical boundary [1,6,10]. In Ladd's shell model, this net mass transfer is canceled out by applying the same moving boundary treatment for both the interior fluid and exterior fluid. For models without interior fluid, the net mass transfer through the boundary exists.

Nguyen and Ladd [10] show that the mass transfer across the solid surface in a time step Δt is recovered when the particle moves to its new position. Our simulations also confirm that although the total mass of the fluid is fluctuating, the total fluid mass drift is very small from a long-term view.

The additional term in Eq. (9) can be interpreted as the fluid mass being covered (or uncovered) at each time step along a boundary link and being injected back to (or down from) the fluid field via Eq. (9). As shown in Fig. 6, after one time step, the wall moves towards the fluid region and arrives at its new position. A small amount of fluid area at $t = t_0$ is covered by solid at $t = t_0 + \Delta t$, while the solid-fluid node map has not changed (for example, node B remains a solid node and node E remains a fluid node). The original fluid in this newly covered area is injected back to the fluid region via the mass flux term, $-2\omega_\alpha \rho \frac{\boldsymbol{e}_\alpha \cdot \boldsymbol{u}_w}{c_s^2}$, by Eq. (9) or (10). More specifically, a unit length wall covers a fluid area of $U_{\mathrm{wall}-x}$ during one time step, and the fluid mass of this area is $\rho_f U_{\mathrm{wall}-x}$. The net mass transfer along link BD, BE, and BF is $6\rho_f w_2 (U_{\mathrm{wall}-x} + U_{\mathrm{wall}-y})$, $6\rho_f w_1 U_{\mathrm{wall}-x}$, and $6\rho_f w_8 (U_{\mathrm{wall}-x} - U_{\mathrm{wall}-y})$, respectively. Thus, the total net fluid mass transfer through the wall from node B during one time step is $\rho_f U_{\mathrm{wall}-x}$, which is exactly the amount of fluid mass of the fluid area being covered by the unit length wall during one time step. The analysis of the fluid node uncovering process is similar to the analysis of the above fluid node covering process.

With the above observation in mind, the problem in the conventional ME method is obvious. The actual momentum exchange along each boundary link is obtained by calculating the momentum difference of the outgoing fluid particles and ingoing fluid particles. The initial macroscopic velocity of the net mass transfer, $-2\omega_\alpha \rho \frac{\boldsymbol{e}_\alpha \cdot \boldsymbol{u}_w}{c_s^2}$, is approximately the velocity of the solid wall but not zero as long as the wall is moving. The conventional ME method does not count in the initial momentum of the net mass transfer, $(-2\omega_\alpha \rho \frac{\boldsymbol{e}_\alpha \cdot \boldsymbol{u}_w}{c_s^2})\boldsymbol{u}_w$. As a result, the impulse force has to be applied to the conventional ME method as a correction. This could also be the cause of nonshell models with the conventional ME method breaking Galilean invariance.

Then it is straightforward to correct the conventional ME method by simply accounting for the initial momentum of the net mass transfer,

$$\delta \boldsymbol{F}_w(\boldsymbol{x}_w, \boldsymbol{e}_\alpha) = -\{f_{\bar{\alpha}}(\boldsymbol{x}_f, t)\boldsymbol{e}_{\bar{\alpha}} - [\tilde{f}_{\bar{\alpha}}(\boldsymbol{x}_f, t)\boldsymbol{e}_\alpha + \Delta \boldsymbol{M}]\}, \tag{30}$$

where $\Delta \boldsymbol{M}$ is the initial momentum of the net mass transfer,

$$\Delta \boldsymbol{M} = \left(-2\omega_\alpha \rho \frac{\boldsymbol{e}_\alpha \cdot \boldsymbol{u}_w}{c_s^2}\right)\boldsymbol{u}_w. \tag{31}$$

The mass flux term $-2\omega_\alpha \rho \frac{\boldsymbol{e}_\alpha \cdot \boldsymbol{u}_w}{c_s^2}$ in Eq. (31) is already obtained in the nonslip boundary condition procedure, and thus the extra computation cost of $\Delta \boldsymbol{M}$ is negligible.

TABLE II. Notations of additional lattice Boltzmann-based methods used in particle sedimentation simulations in Sec. V.

Method	Boundary condition	Force evaluation	Impulse force	Interior fluid
CB-CME-present	Curved boundary	CME present	No	No
CB-CME-Caiazzo	Curved boundary	CME in Ref. [36]	No	No
BB-CME-present	Midway bounce-back	CME present	No	No
BB-CME-Caiazzo	Midway bounce-back	CME in Ref. [36]	No	No

The impulse force proposed in Ref. [8] then can be explained. As shown in Fig. 6, after one time step, the sum of the corrected term $\Delta \boldsymbol{M}$ in Eq. (30) from node B is $\rho_f U_{\text{wall}-x} \boldsymbol{U}_{\text{wall}}$, which is exactly the initial momentum of the fluid being covered by the unit length wall during one time step. When the wall moves from node B to node E, and the wall velocity and fluid density are assumed to be constant, then the total initial momentum of the newly coved fluid area by a unit length wall during this period is $\rho_f \boldsymbol{U}_{\text{wall}}$. Thus, the total impulse generated from the impulse force defined in Eqs. (25) and (27) is equal to the total initial momentum of the fluid mass that the unit length wall covers or uncovers during the period that the wall moves from one lattice node to a neighboring lattice node as shown in Fig. 6. By using our method, Eq. (30), the above initial momentum is smoothly accounted for, which is more physical and stable compared to the impulse force correction.

Caiazzo and Junk [36] proposed an alternative modified ME method based on asymptotic analysis,

$$\delta \boldsymbol{F}_w(\boldsymbol{x}_w, \boldsymbol{e}_\alpha) = \delta \tilde{\boldsymbol{F}}_w(\boldsymbol{x}_w, \boldsymbol{e}_\alpha) - 2w_\alpha \boldsymbol{e}_\alpha - \rho w_\alpha c_s^{-2} \left\{ c_s^{-2} |\boldsymbol{e}_\alpha \cdot \boldsymbol{u}_w|^2 - \boldsymbol{u}_w^2 \right\} \boldsymbol{e}_\alpha, \quad (32)$$

where $\delta \tilde{\boldsymbol{F}}_w(\boldsymbol{x}_w, \boldsymbol{e}_\alpha)$ is the force obtained by Eq. (14). Clausen and Aidun [37] derived a similar formula and correct the method by creating an internal boundary node so that the effect of the error term in the conventional ME method could be canceled out. The second term in the RHS of Eq. (32) simply represents the hydrostatic pressure [37]. Their method, Eq. (32), was proved to be Galilean invariant via a numerical simulation of a single particle crossing Lees-Edwards boundary [38] and a shear flow test [37], while the improvement in more practical simulations, such as particle sedimentation, was not shown. In the following section, their method will also be compared with our method.

V. RESULTS AND DISCUSSION

In this section the corrected ME methods are put into test. In Table II CME-present stands for the corrected ME method proposed in this paper, and CME-Caiazzo stands for the corrected ME method proposed in Ref. [36]. The notations of other methods are shown in Table I.

A. Accuracy tests

1. A moderate Reynolds number case with $Re = 6.6$

The $\text{Re} = 6.6$ sedimentation case in Sec. III is once again adopted to validate our new momentum exchange method. In Sec. III, we find that the results from CB-ME, BB-ME, CB-SI-IMP, and VF are inaccurate, and those results will not be presented here.

We can see from Fig. 7 that both CB-CME-present and CB-CME-Caiazzo agree well with FEM and CB-SI. A similar conclusion can be made for the methods using the midway bounce-back boundary condition, as shown in Fig. 8. Compared with CB-ME-IMP and BB-ME-IMP, the impulse force is no longer required in our corrected ME method, thus the force acting on the particle is much smoother and comparable with force obtained by the SI method, as shown in Fig. 9. Figure 9 also shows that the advantage of using the curved boundary condition is preserved, as the force obtained by the curved boundary condition is smoother than the force obtained by the midway bounce-back boundary condition. Although VF does not produce accurate trajectory and orientation of the particle in this case, VF does produce the smoothest force in all the methods tested in this paper. The difference between results of our method (CME-present) and the corrected ME method (CME-Caiazzo) proposed in Ref. [36] is negligible.

2. Two relatively low Reynolds number cases with $Re = 0.31$ and $Re = 0.82$, respectively

In order to further evaluate the methods, the $\text{Re} = 0.82$ and the $\text{Re} = 0.31$ cases are carried out. These two cases have also been adopted in Ref. [3], and FEM data are available in Ref. [31].

The geometries of the $\text{Re} = 0.82$ and $\text{Re} = 0.31$ cases are the same and shown in Fig. 2. The computation domain is a closed channel. In the lattice unit, the channel width L is 100, and the channel length is $30L$. The particle is initially placed at the center of the channel and is $3L$ away from the end of the channel in the negative direction of the x axis, with $\theta = 135^\circ$. $a = 1.5b = 10$ and τ is chosen to be 0.6. The solid-fluid density ratio is 1.005 and 1.0015 for the $\text{Re} = 0.82$ case and $\text{Re} = 0.31$ case, respectively.

The physical parameters are not available for the two cases here, while only the solid-fluid density ratio, terminal Reynolds number, and initial and terminal particle orientation are known. Thus, gravity (in lattice units) is adjusted to ensure the terminal Reynolds number and orientation match with the FEM data. Our simulations show that $g = 1.355 \times 10^{-3}$ is good for all the methods tested here, except for LBM with the SI method, in which $g = 1.375 \times 10^{-3}$. However, for these two low Reynolds number cases, the actual differences of simulation results obtained by the two gravity values is relatively small and have no significant influence on the final conclusion. Thus, only results of $g = 1.355 \times 10^{-3}$ are shown here.

In Fig. 10 both CB-ME-IMP and VF agree well with FEM, while CB-SI slightly deviates from FEM and all other LBM results in the $\text{Re} = 0.31$ case, which indicates that the stress integration method is not accurate in this particular low

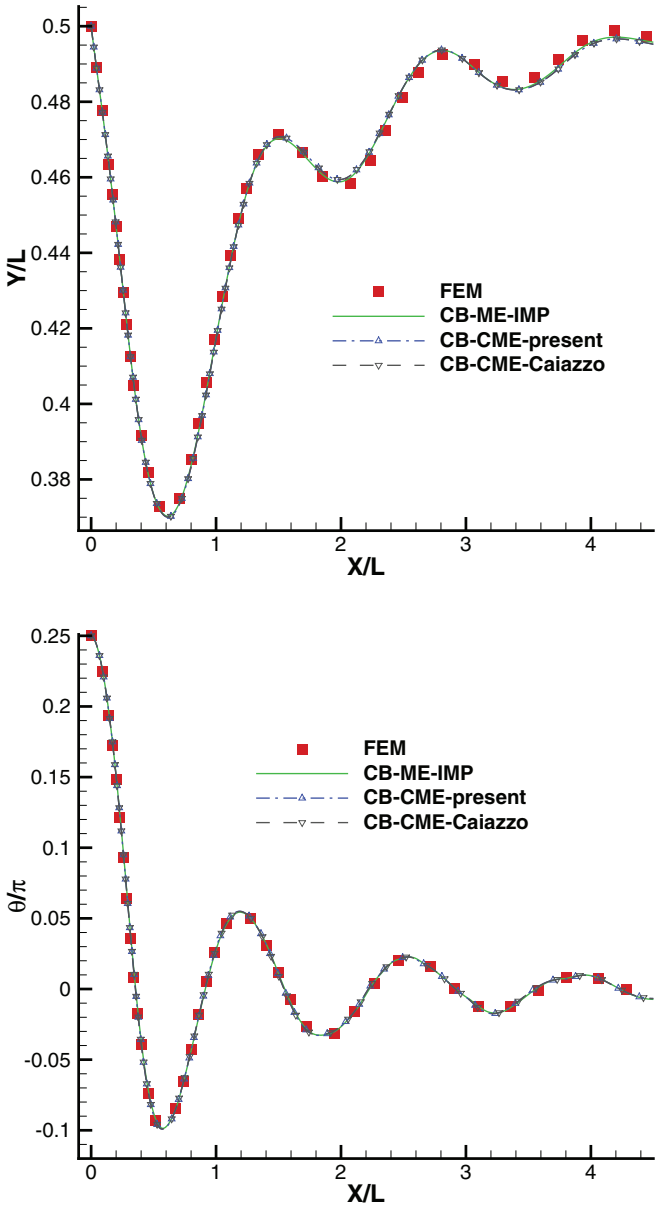

FIG. 7. (Color online) Comparison of particle trajectories and orientations for the Re = 6.6 case obtained by FEM [5] and LBM with the curved boundary condition. Results of the two corrected ME methods, CB-CME-present and CB-CME-Caiazzo, are included and show good agreement with the FEM data. The difference between results of our method (CB-CME-present) and the corrected ME method (CB-CME-Caiazzo) proposed in Ref. [36] is negligible.

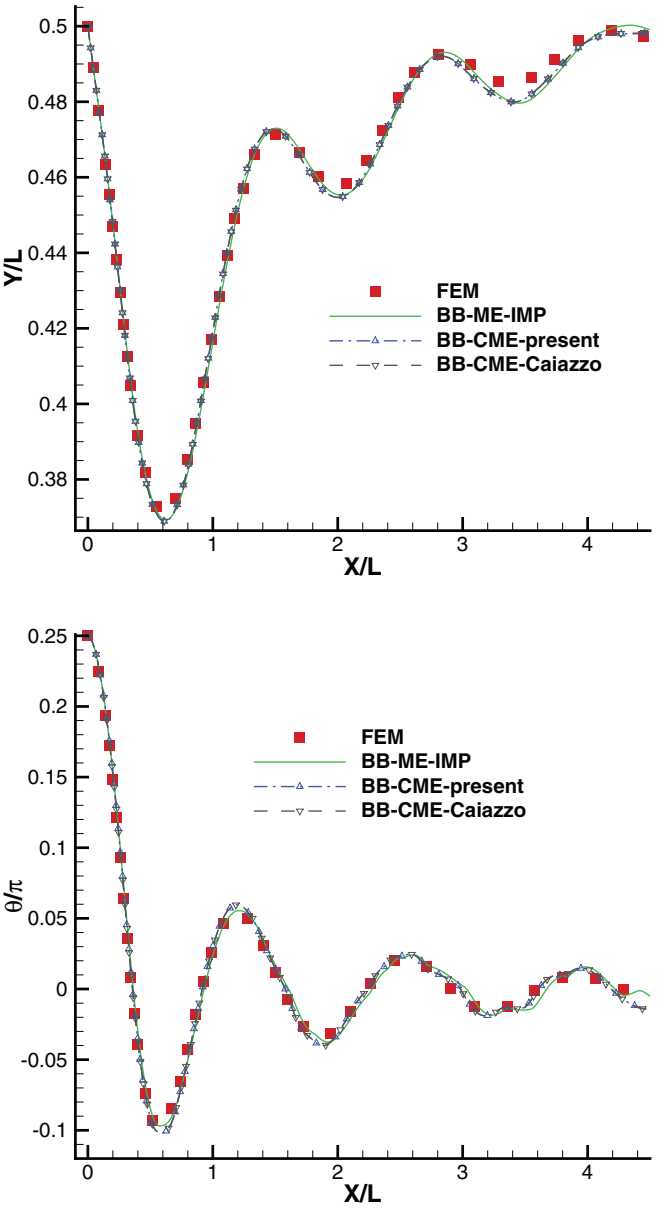

FIG. 8. (Color online) Comparison of particle trajectories and orientations for the Re = 6.6 case obtained by FEM [5] and LBM with the midway bounce-back boundary condition. Results of the two corrected ME methods, BB-CME-present and BB-CME-Caiazzo, are included and show good agreement with the FEM data. The difference between results of our method (BB-CME-present) and the corrected ME method (BB-CME-Caiazzo) proposed in Ref. [36] is negligible.

Reynolds number case. The results by CB-CME-present and CB-CME-Caiazzo are shown in Fig. 11, both of which are almost identical to CB-ME-IMP and agree well with FEM.

3. *A relatively high density ratio case with Re = 11*

In the Re = 6.6, Re = 0.82, and Re = 0.31 cases, the solid-fluid density ratio is relatively small, which is not suitable for the shell model. Here we use the same simulation setup in the Re = 6.6 case, except that the density ratio is raised to 3.0 instead of 1.1 in the Re = 6.6 case, and the fluid viscosity is also raised to 3.0×10^{-6} m^2/s. Under this setup, the terminal Reynolds number is 11 (the Re = 11 case), which is valid for either using the ME method or the SI method.

Since there are no FEM data available in this case, in order to obtain an accurate result for comparison, we refine the grid so that the resolution becomes 520 grid cells per cm, compared with 260 grid cells per cm before grid refining. Figure 12 shows the fine grid results. All the methods tested here show very good agreement with each other, except VF, which deviates significantly from other methods. In the Re = 6.6 case, VF also deviates from other results including FEM and is considered to be inaccurate. Thus, the fine grid CB-CME-present data

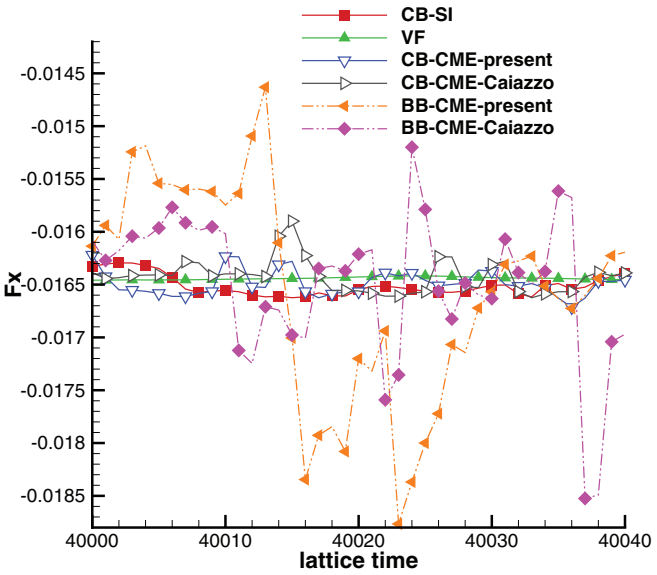

FIG. 9. (Color online) Comparison of fluid force acting on the particle during the terminal settling state for the Re = 6.6 case obtained by LBM. Results of the two corrected ME methods are included and comparable with the results of the SI method in terms of smoothness. Forces obtained by BB-CME-present and BB-CME-Caiazzo still fluctuate in some degree mainly due to the midway bounce-back boundary condition. Readers should keep in mind that the scale of F_x in this figure is different from the one in Fig. 5.

is adopted as the benchmark for comparison in the following normal grid resolution (260 grid cells per cm) test.

Figure 13 shows results obtained by the curved boundary condition and the volume fraction model with normal grid resolution. VF again deviates from other methods. Due to reduced grid resolution, as the particle approaches the terminal state in the middle of the channel, results of different methods begin to deviate a little from each other and the fine grid result but still in an acceptable range. Figure 14 shows results obtained by the midway bounce-back boundary condition with normal grid resolution. The result by Ladd's shell model is also included for comparison. The midway bounce-back boundary condition is first-order accurate for arbitrary surface, and the Reynolds number in this case is relatively high. However, results obtained by the midway bounce-back boundary condition still agree well with the fine grid result from CB-CME-present, although not as well as the curved boundary condition results when the particle approaches to the terminal state in the middle of the channel. The shell model is as accurate as other methods that employ the midway bounce-back boundary condition in this case.

B. Galilean invariance

Several papers have studied the Galilean invariance of the particle suspension models [36–38]. The benchmark case in Ref. [37] is adopted to evaluate our new corrected momentum exchange method, as well as other methods used in this paper. For simplicity, the benchmark case is modified into two-dimensional case.

The geometry of the case is shown in Fig. 15. The periodic boundary condition is applied to the inlet and outlet

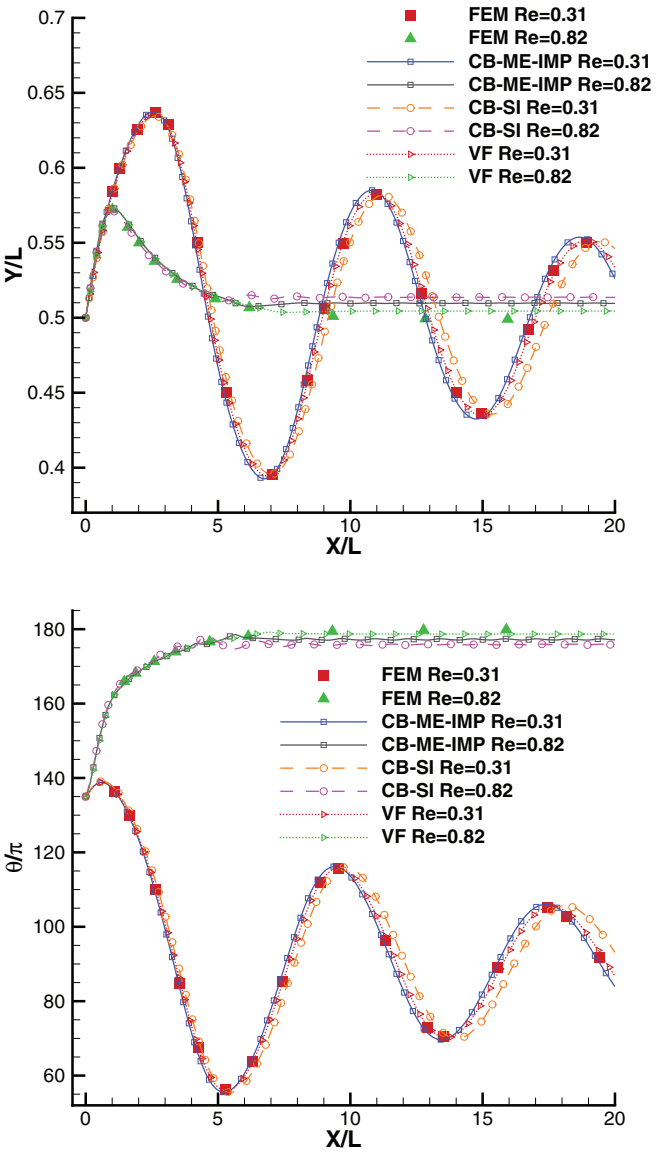

FIG. 10. (Color online) Comparison of particle trajectories and orientations for the Re = 0.82 case and the Re = 0.31 case obtained by FEM [31] and LBM with the curved boundary condition. CB-SI slightly deviates from FEM in the Re = 0.31 case, while other LB-based methods agree well with FEM, which indicates that the stress integration method is not accurate in this particular low Reynolds number case. Among all the LB-based methods, VF has best match with FEM.

of the channel. The computation domain is 100 × 500. The two-dimensional circular particle which has a radius of 10 lattice units is initially placed in the middle of the channel and is 100 lattice units away from the inlet of the channel. The solid-fluid density ratio is 3.0 and τ is 0.6. Initial velocity of the fluid is $U_x + \dot{\gamma} H/2 - \dot{\gamma} y$, where $\dot{\gamma}$ is the shear rate and y is the distance from the bottom wall. The particle is also assigned with a initial translational velocity of U_x and is allowed only to move in the x direction. The physical system of this case is Galilean invariant. Thus, the particle should experience negligible y direction force if the numerical simulations are Galilean invariant.

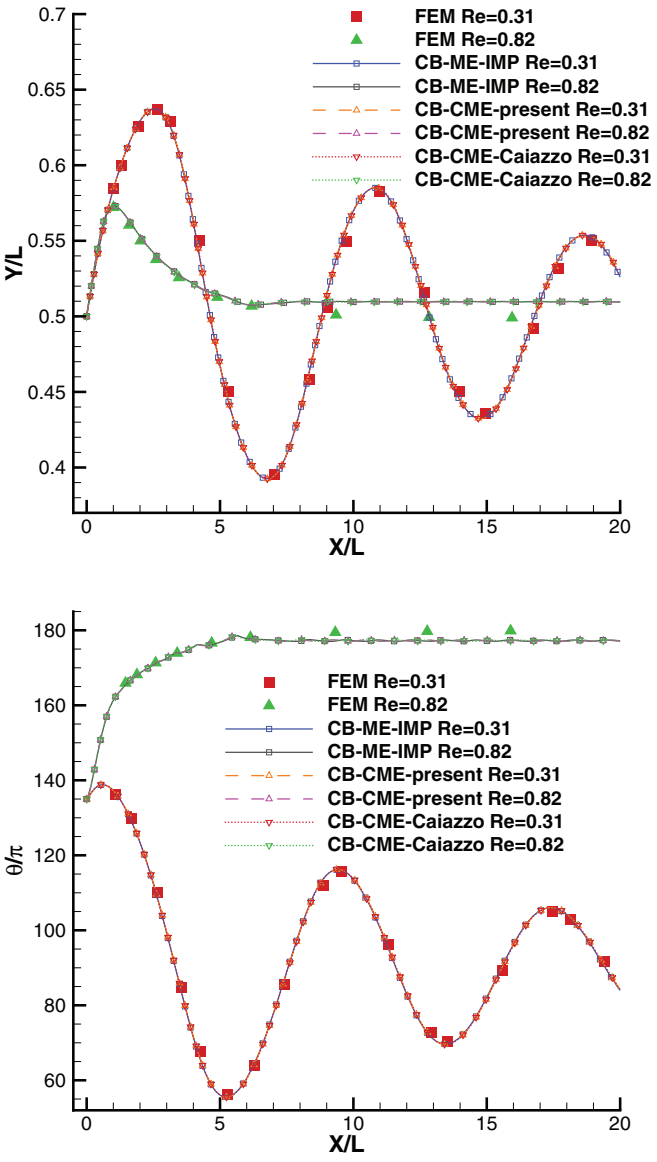

FIG. 11. (Color online) Comparison of particle trajectories and orientations for the Re = 0.82 case and the Re = 0.31 case obtained by FEM [31] and LBM with the curved boundary condition. Results by the two corrected momentum exchange methods, CB-CME-present and CB-CME-Caiazzo, are included and show good agreement with the FEM data.

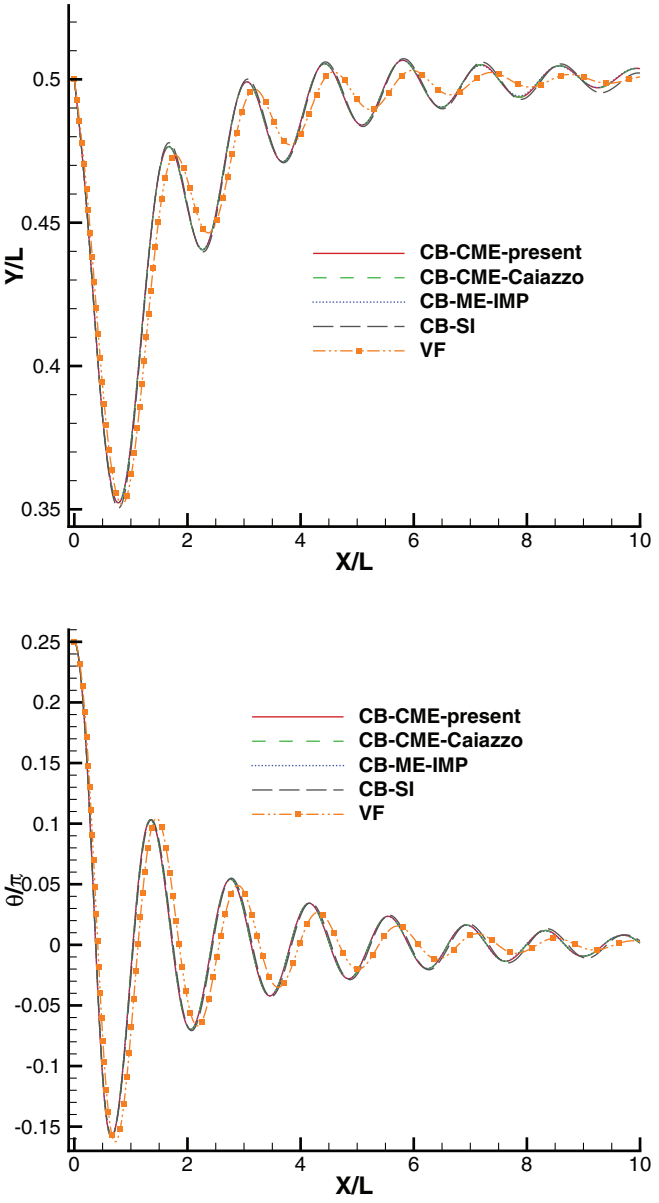

FIG. 12. (Color online) Comparison of particle trajectories and orientations for the high-density ratio Re = 11 case obtained by LBM with the curved boundary condition using a fine grid resolution (520 lattice units per cm). All the methods tested here show very good agreement with each other, except VF, which deviates significantly from other methods.

We follow the work of Ref. [37] and vary the value of U_x and $\dot{\gamma}$ separately. In Fig. 16 the translational velocity $U_x = 0.01$ and is kept constant, while the shear rate $\dot{\gamma}$ is varied. In Fig. 17 the shear rate $\dot{\gamma} = 2.5 \times 10^{-5}$ and is kept constant, while the translational velocity U_x is varied. As shown in Fig. 9, even without the impulse force in Eq. (25) and in Eq. (27), the fluid force acting on the particle obtained by LBM still fluctuates to some degree. Thus, the y direction force F_y discussed below is averaged during the period the particle moves within $x = (200, 300)$ in the channel.

The conventional ME method without correction results in a relatively large F_y and hence breaks Galilean invariance. The magnitude of F_y of CB-ME or BB-ME increases linearly as $U_x\dot{\gamma}$ increases, as shown in both Figs. 16 and 17, which indicates that F_y is linearly related to both translational velocity and shear rate.

With either correction proposed in this paper or in Ref. [36], F_y is two orders of magnitude smaller than the one without correction; thus we can claim that our corrected ME method is Galilean invariant. In the shell model, as the interior fluid interacts with the boundary in the same way as the exterior fluid, the consequence of not accounting for the initial momentum of the mass transfer in Eq. (9) is canceled out, and no correction is required. For the SI method and the volume fraction model, force evaluation does not involve the miscalculation of the momentum exchange in the conventional ME equation, and thus both methods should be Galilean

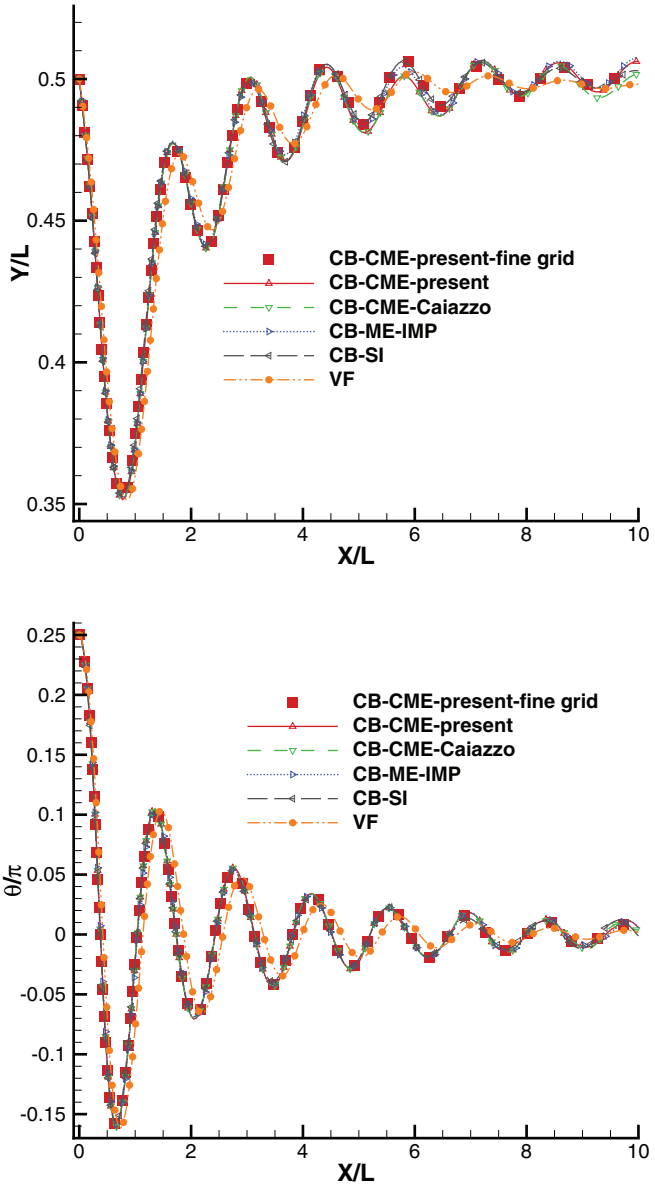

FIG. 13. (Color online) Comparison of particle trajectories and orientations for the high-density ratio Re = 11 case obtained by LBM with the curved boundary condition using a normal grid resolution (260 lattice units per cm). All the LB-based methods agree well with each other and the fine grid result, except the VF result, which deviates from the fine grid result significantly. Thus, VF is not accurate in this case.

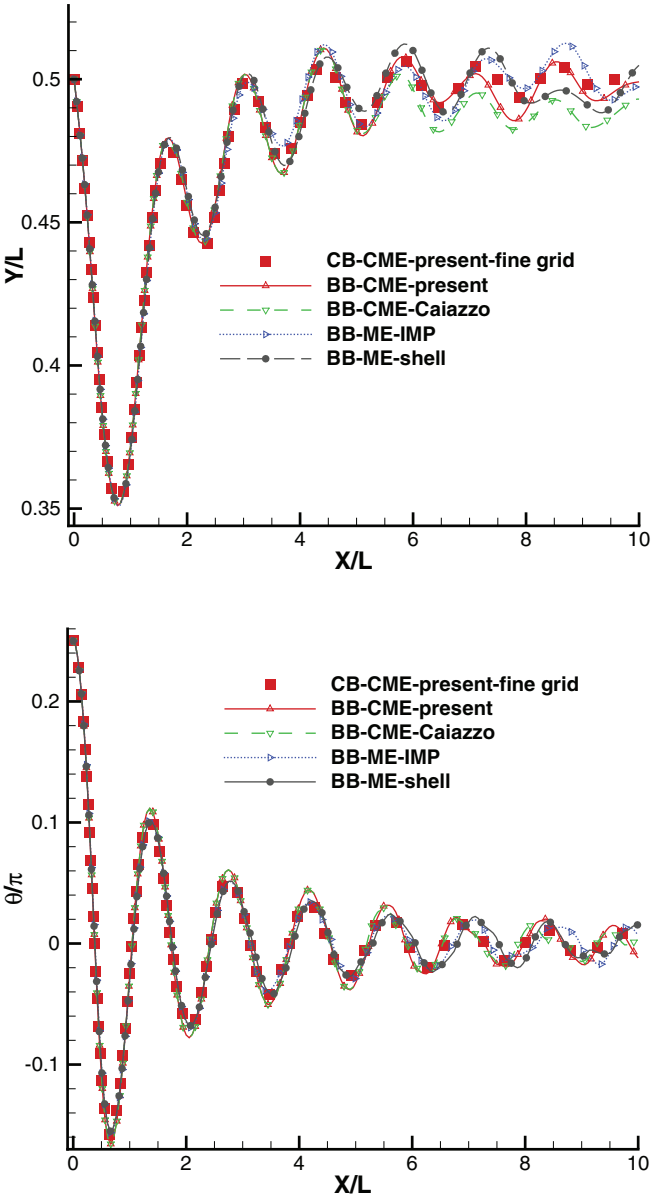

FIG. 14. (Color online) Comparison of particle trajectories and orientations for the high-density ratio Re = 11 case obtained by LBM with the curved boundary condition using a normal grid resolution (260 lattice units per cm). All the LB-based methods agree well with each other and the fine grid result, although not as well as the results obtained by LBM using the higher-order curved boundary condition. BB-ME-shell is as accurate as other methods that employ the midway bounce-back boundary condition in this case.

invariant. Our simulations show that F_y of the shell model, volume fraction model, and LBM with the SI method is two to three orders of magnitude smaller than F_y of CB-ME, which agrees with our analysis.

C. Efficiency

Although the SI method requires a lot of extrapolations and, as a result, is definitely more time consuming than the ME method, one may be interested in the exact difference of efficiency between the two methods. The Re = 6.6 sedimentation case is chosen for efficiency comparison. The simulations are run on a desktop computer equipped with an Intel I7 3770 CPU (3.4 GHz). The Turbo Boost feature of the CPU is disabled in order to run these simulations under the same CPU frequency. The code is written in FORTRAN and compiled with the Intel Visual Fortran Composer XE 2013 with OpenMP disabled. Due to the execution of the ME method being extremely fast and the ME method embedded in the boundary condition treatment, the computation time of the ME method is difficult to measure. A preliminary test with the particle moving at a constant speed (hence force evaluation is irrelevant) shows that the difference between the computation time of the whole particle treatment segment with or without

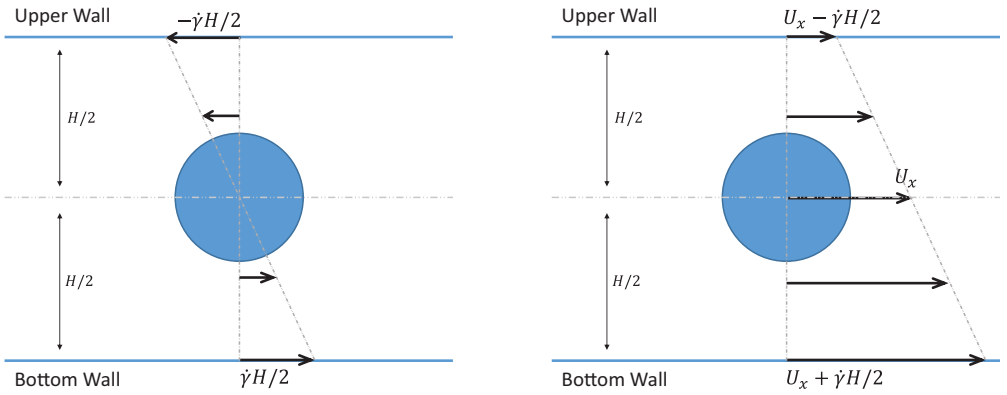

FIG. 15. (Color online) The geometry of the Galilean invariance benchmark case. $\dot{\gamma}$ is the shear rate. Periodic boundary condition is applied to the inlet and outlet of the channel. In the left figure, the translational velocity U_x is zero, and the particle will rotate under shear flow with no translational velocity. In the right figure, the whole fluid phase and solid phase system is applied with a constant translational velocity U_x. The physical system is Galilean invariant, and the particle will stay in the middle of the channel and experience no vertical fluid force.

the ME method being executed is barely noticeable. Thus, we monitor only the stress integration segment of the code as well as the whole particle treatment segment, which involves the particle boundary treatment, force evaluation, and the particle velocity and position update. The ME segment is assumed to be negligible compared with the whole particle treatment segment.

The averaged (averaged from $t = 10\,000$ to $t = 60\,000$) computation time of the particle treatment segment and the SI segment per 1000 time steps is shown in Table III. The SI segment alone costs about three times more computation time than the whole particle treatment segment when using the ME method. For the SI method used here, the integral of Eq. (18) is approximated by the quadrature of 400 points, which is also adopted in several other papers [5,19,29]. The computation time can be reduced by using fewer points for integration; however, the accuracy of stress integration method may also be reduced. Nevertheless, the ME method requires significantly less computation time than the SI method. The computation of an accurate solid volume fraction of a lattice cell is time consuming, thus the computation cost of VF is much higher than those link-based LB methods. In Table III the computation time of the particle treatment segment of CB-CME-present is just about twice the computation time of BB-CME-present; thus, the extra cost of the curved boundary condition compared to the bounce-back boundary condition is acceptable. For dilute particle suspensions, the curved boundary condition is promising since it brings in subgrid resolution without too much extra computation cost.

In summary, the two corrected momentum exchange methods without the impulse force are promising in the lattice Boltzmann simulations of particle-fluid interactions. Compared with the conventional ME method with the impulse force correction, the two corrected ME methods do not require us to apply the impulse force whenever the particle moves to cover or uncover a fluid node; thus, the total force obtained by the corrected ME methods is much smoother. Compared with

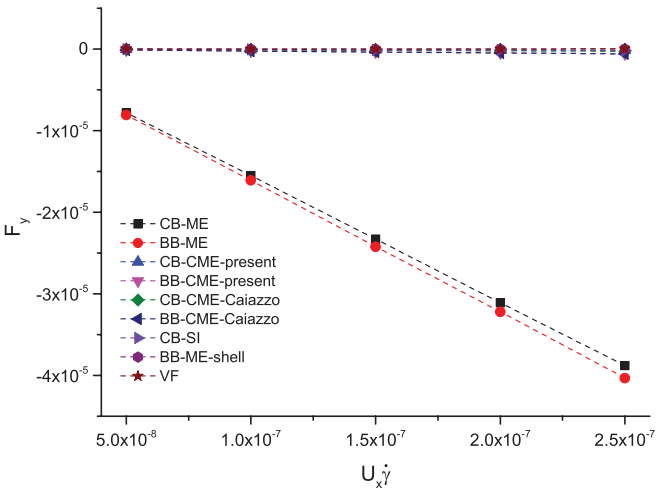

FIG. 16. (Color online) Force error for the circular particle in the shear flow test. The translational velocity U_x is kept constant at 0.01. Simulations employing the conventional ME method, CB-ME and BB-ME, result in significant vertical force compared to other methods.

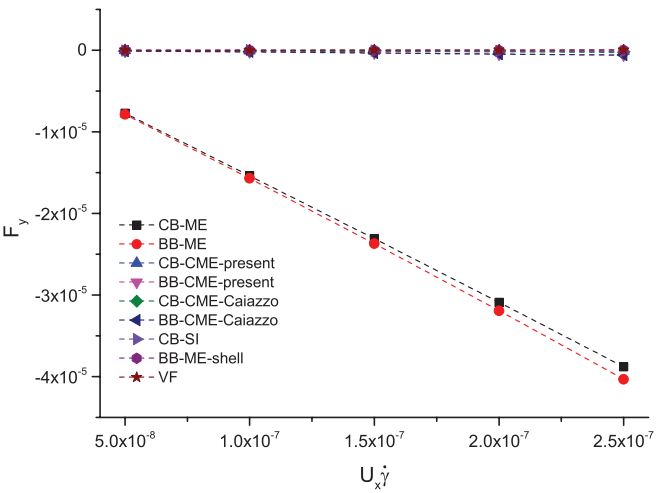

FIG. 17. (Color online) Force error for the circular particle in the shear flow test. The shear rate $\dot{\gamma}$ is kept constant at 2.5×10^{-5}. Simulations employing the conventional ME method, CB-ME, and BB-ME result in significant vertical force compared to other methods.

TABLE III. Averaged computation time of the whole particle treatment segment and the force evaluation segment per 1000 time steps for a single particle

Method	Particle treatment segment	Force evaluation segment
CB-SI	0.288s	0.235s
CB-CME-present	0.058s	<0.001s
BB-CME-present	0.030s	<0.001s
VF	1.055s	0.013s

the SI method, the total force obtained by the corrected ME methods is as smooth as the SI method, while the computation cost is much lower than the SI method. Also, the corrected ME methods are interpolation or extrapolation free, which is critical for dense particle suspensions where there is not enough information available for the extrapolations required in the SI method.

Although the corrected momentum exchange method in Ref. [36] has been proposed since 2008, the latest papers on particle suspensions are still using the impulse force correction [12,14,21]. The reason is probably that the previous studies mainly focus on Galilean invariance [36–38], while the impact on the real world simulations is not well presented. Also the physical meaning of the correction term is not well explained, which may confuse users, as the momentum exchange method is proved to be quite accurate in the still walls test [28]. Compared with the corrected ME method in Ref. [36], both methods obtain almost identical simulation results, while our method is based on the definition of the momentum exchange, the momentum difference of the ingoing and outgoing fluid particles along the boundary link, and provides detailed interpretation of the correction term, which is also helpful for the design of new lattice Boltzmann particle suspension models. Nevertheless, both corrected momentum exchange methods are superior to the impulse force correction and deserve further investigation.

VI. CONCLUSIONS

In this work, the physical cause of the inaccurate particle dynamics obtained by lattice Boltzmann simulations using the conventional momentum exchange method without correction is revealed. In the moving boundary treatment, a net fluid mass transfer through the physical boundary exists due to the fixed discretized lattice velocity. The physical interpretation of the net mass transfer is that a small portion of fluid region is covered (or uncovered) by the moving solid wall in each time step and the fluid mass of this region is injected back to (or down from) the fluid region at the same time. The conventional momentum exchange method does not account for the initial momentum of the net mass transfer in the moving boundary treatment, and the force evaluated from the momentum exchange method is thus inaccurate once the wall is moving towards the fluid. An impulse force was proposed to modify the force evaluation whenever the particle moves to cover or uncover a lattice node, but led to significant fluctuation of force and reduced simulation stability. We propose a corrected momentum exchange method by accounting for the initial momentum of the net mass transfer. This method is easy to implement with negligible extra computational costs, and the impulse force is no longer required. Direct numerical simulations of a single elliptical particle sedimentation are carried out to evaluate different lattice Boltzmann-based methods for particle-fluid interactions, including the corrected momentum exchange method proposed in this paper, by comparisons with results from the finite element method. Based on the results and analysis, we conclude the following:

(1) The simulation results using our corrected momentum exchange method agree well with the FEM data for all the numerical cases in this paper. As no impulse force is required, the force evaluated by our method is as smooth as that of the stress integration method. The correction is local with negligible additional computation costs. Our method is valid for both the midway bounce-back boundary condition and the curved boundary treatments and is Galilean invariant.

(2) The stress integration method for force evaluation in LBM can lead to accurate and stable particle dynamics and needs no impulse force correction. However, it requires a huge amount of extrapolations, which results in high computation costs. The implementation of the stress integration method will be very complicated for three-dimensional simulations. Our numerical results show that for the relatively low Reynolds number, such as the case of $\mathrm{Re} = 0.31$, the stress integration method slightly deviates from both FEM and other LB-based methods. Various factors may affect the accuracy of the stress integration method, such as the extrapolation scheme and the exact integration surface, and further investigation is necessary.

(3) Forces on the particle obtained by the volume-fraction LB method are the smoothest among all the methods tested in this paper. The volume fraction model agrees well with FEM in the relatively lower Reynolds number cases, but deviates from that for higher Reynolds number cases. Nonrigid behavior of the interior fluid may be responsible. The computation cost to obtain accurate solid volume fraction of a lattice cell is very high, which further limits the use of this method.

ACKNOWLEDGMENT

This work is financially supported by the National Natural Science Foundation of China (Grant No. 51176089, 91130001) and the National Key Basic Research Program of China (Grants No. 2013CB228301, No. 2009CB724101).

[1] C. K. Aidun and J. R. Clausen, Annu. Rev. Fluid Mech. **42**, 439 (2010).

[2] J. Li, *Particle-Fluid Two-Phase Flow: The Energy-Minimization Multi-scale Method* (Metallurgical Industry Press, Beijing, 1994).

[3] D. W. Qi, J. Fluid Mech. **385**, 41 (1999).

[4] P. Bolhuis, A. Louis, J. Hansen, and E. Meijer, J. Chem. Phys. **114**, 4296 (2001).

[5] Z. Xia, K. W. Connington, S. Rapaka, P. Yue, J. J. Feng, and S. Chen, J. Fluid Mech. **625**, 249 (2009).

[6] A. J. C. Ladd, J. Fluid Mech. **271**, 285 (1994).
[7] A. J. C. Ladd, J. Fluid Mech. **271**, 311 (1994).
[8] C. K. Aidun, Y. N. Lu, and E. J. Ding, J. Fluid Mech. **373**, 287 (1998).
[9] A. J. C. Ladd and R. Verberg, J. Stat. Phys. **104**, 1191 (2001).
[10] N. Q. Nguyen and A. J. C. Ladd, Phys. Rev. E **66**, 046708 (2002).
[11] C. P. Lowe, D. Frenkel, and A. J. Masters, J. Chem. Phys. **103**, 1582 (1995).
[12] F. Jansen and J. Harting, Phys. Rev. E **83**, 046707 (2011).
[13] X. Yin, G. Le, and J. Zhang, Phys. Rev. E **86**, 026701 (2012).
[14] B. Wen, H. Li, C. Zhang, and H. Fang, Phys. Rev. E **85**, 016704 (2012).
[15] O. Filippova and D. Hanel, J. Comput. Phys. **147**, 219 (1998).
[16] R. W. Mei, L. S. Luo, and W. Shyy, J. Comput. Phys. **155**, 307 (1999).
[17] M. Bouzidi, M. Firdaouss, and P. Lallemand, Phys. Fluids **13**, 3452 (2001).
[18] P. Lallemand and L. S. Luo, J. Comput. Phys. **184**, 406 (2003).
[19] H. Li, X. Lu, H. Fang, and Y. Qian, Phys. Rev. E **70**, 026701 (2004).
[20] K. Connington, Q. Kang, H. Viswanathan, A. Abdel-Fattah, and S. Chen, Phys. Fluids **21**, 053301 (2009).
[21] H. B. Huang, X. Yang, M. Krafczyk, and X. Y. Lu, J. Fluid Mech. **692**, 369 (2012).
[22] Y. H. Qian, D. Dhumieres, and P. Lallemand, Europhys. Lett. **17**, 479 (1992).
[23] H. D. Chen, S. Y. Chen, and W. H. Matthaeus, Phys. Rev. A **45**, R5339 (1992).
[24] S. Chen and G. D. Doolen, Annu. Rev. Fluid Mech. **30**, 329 (1998).
[25] M. Wang and S. Chen, J. Colloid Interf. Sci. **314**, 264 (2007).
[26] R. Mei, W. Shyy, D. Yu, and L.-S. Luo, J. Comput. Phys. **161**, 680 (2000).
[27] D. Yu, Prog. Aerosp. Sci. **39**, 329 (2003).
[28] R. Mei, D. Yu, W. Shyy, and L.-S. Luo, Phys. Rev. E **65**, 041203 (2002).
[29] T. Inamuro, K. Maeba, and F. Ogino, Int. J. Multiphase Flow **26**, 1981 (2000).
[30] J. Feng, H. H. Hu, and D. D. Joseph, J. Fluid Mech. **261**, 95 (1994).
[31] P. Y. Huang, H. H. Hu, and D. D. Joseph, J. Fluid Mech. **362**, 297 (1998).
[32] T. N. Swaminathan, K. Mukundakrishnan, and H. H. Hu, J. Fluid Mech. **551**, 357 (2006).
[33] D. R. Noble and J. R. Torczynski, Int. J. Mod. Phys. C **9**, 1189 (1998).
[34] Z. G. Feng and E. E. Michaelides, J. Comput. Phys. **195**, 602 (2004).
[35] B. K. Cook, D. R. Noble, and J. R. Williams, Eng. Comput. **21**, 151 (2004).
[36] A. Caiazzo and M. Junk, Comput. Math. Appl. **55**, 1415 (2008).
[37] J. R. Clausen and C. K. Aidun, Int. J. Multiphase Flow **35**, 307 (2009).
[38] E. Lorenz, A. Caiazzo, and A. G. Hoekstra, Phys. Rev. E **79**, 036705 (2009).